ACS APPLIED MATERIALS & INTERFACES

Research Article

www.acsami.org

# High-Performance UV Photodetection of Unique ZnO Nanowires from Zinc Carbonate Hydroxide Nanobelts

Lu Ren,[†] Tingting Tian,[†] Yuanzhi Li,*[,†] Jianguo Huang,[‡] and Xiujian Zhao[†]

[†]State Key Laboratory of Silicate Materials for Architectures, Wuhan University of Technology, 122 Luoshi Road, Wuhan 430070, P.R. China

[‡]Department of Chemistry, Zhejiang University, Hanzhou, Zhejiang 310027, P.R. China

**ABSTRACT:** Zinc carbonate hydroxide nanobelts are prepared by the hydrolysis of zinc acetate aqueous solution in the presence of urea at 90 °C. The zinc carbonate hydroxide nanobelts can be facilely self-assembled in a circular flexible freestanding film with a diameter of 8.4 cm and thickness of ~48 μm. The calcination of the zinc carbonate hydroxide nanobelts at 300 °C under normal atmospheric condition results in the formation of ZnO nanowires. The zinc carbonate hydroxide nanobelts and resultant ZnO nanowires are characterized by XRD, SEM, TEM, TG-DSC, PL, and impedance measurement. The characterization results indicate that the ZnO nanowires exhibit unique nanostructure characterized by long chains of closely attached ZnO nanocrystals with ZnO/ZnO nanocrystal junctions. The unique ZnO nanowire-based UV photodetector exhibit much higher photoresponse currents (at the milliampere level) and on/off current ratio (~1000) than ZnO nanocrystal-based UV photodetector. Under the UV irradiance of 120 mW cm$^{-2}$ and low applied voltage of 0.5 V, the peak photoresponse current and on/off current ratio of the ZnO nanowire photodetector are 56 and 36 times higher than those of the ZnO nanocrystal UV photodetector, respectively. The reason for the superior photodetection performance of the ZnO nanowires over the ZnO nanocrystals is discussed.

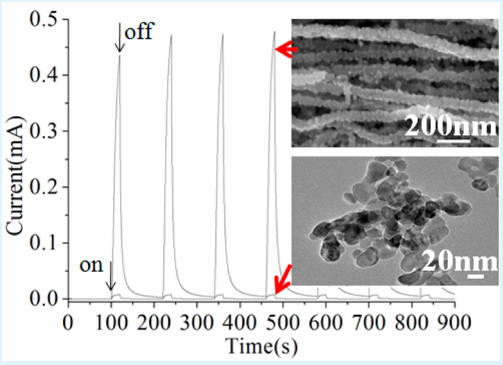


**KEYWORDS:** *ZnO, nanowires, nanobelts, nanocrystals, junctions, photodetector*

## 1. INTRODUCTION

ZnO, a promising functional semiconductor because of its wide direct bandgap (3.37 eV) and large exciton energy (60 meV), relatively low cost, and facilely controllable nano/microstructures, has been extensively investigated for a vast range of applications such as light-emitting diodes,[1] lasers,[2] electrical generators,[3] photovoltaics,[4,5] sensors,[6,7] photocatalyis,[8,9] photodetectors,[10−25] etc. For photodetector applications, high on/off current ratio, fast response and recovery, and large photoresponse current are desirable sensor characteristics.[10,25] Various ZnO nanostructures such as nanoparticle,[11,12] hollow sphere,[13] hollow sphere with double-yolk egg structure,[14] nanobelt,[15] nanorod,[16−18] nanowire,[19−21] and nanoparticle/nanowire complex structure,[22] have been prepared and applied in photodetector. Among the various ZnO nanostructures, one-dimensional ZnO nanostructures such as nanobelt, nanorod, and nanowire are considered as one of the most promising sensitive materials in photodetectors due to the large surface-to-volume ratio, a Debye length comparable to their small size and ideal transport characteristics in terms of the charge carriers.[22−24] The photodetectors constructed from ZnO single nanowire or nanobelt usually show high on/off current ratio and fast response time. However, an essential hindrance to ZnO single nanowire UV photodetectors is the very low photoresponse current due to the small size of individual nanowire or nanobelt. High-precision measurement systems are necessary to detect the signal, making such photodetectors cost prohibitive.[25] Various strategies have been developed to enhance the UV photoresponse current of ZnO single nanowire or nanobelt photodetectors. These strategies include: 1) the decoration of ZnO nanowire with Au, Ag nanoparticles,[26,27] 2) the formation of ZnO nanowire or nanobelt composite with $SnO_2$ or ZnS,[24,28,29] 3) the surface-functionalization of ZnO nanobelt with polymer,[30] etc. The photoresponse currents of the ZnO single nanowire or nanobelt photodetectors enhanced by these strategies are generally at microampere (μA) level. Recently, Mandal et al. demonstrated that the formation of ZnO nanorod array/agarose gel film heterojunction led to an significant enhancement in photoresponse current (at the milliampere (mA) level) as compared to only ZnO nanorod array film because of the electric-field-induced band bending at the interface and the light-harvesting nature of nanorods configuration.[31] Bai et al. reported that the integration of multiple ZnO nanowires connected in parallel could generate enhanced UV photoresponse currents at approximately the milliamp level.[25] Herein, we develop a novel approach to prepare ZnO nanowires with unique nanostructure by the thermal decomposition of the zinc

**Received:** April 29, 2013
**Accepted:** May 23, 2013
**Published:** May 23, 2013

  

carbonate hydroxide nanobelts, which are synthesized by the hydrolysis of zinc acetate aqueous solution in the presence of urea. The unique ZnO nanowires, which are composed of long chains of closely attached ZnO nanocrystals with ZnO/ZnO nanocrystal junctions, exhibits much higher photoresponse current (at approximately the milliamp level) and on/off current ratio as compared to ZnO nanocrystals.

## 2. EXPERIMENTAL METHODS

**2.1. Preparation.** Zinc acetate ($ZnAc_2{\cdot}2H_2O$, 2.216 g) and 1.400 g of urea were dissolved in 100 mL of distilled water by ultrasonication, respectively. The $ZnAc_2$ and urea aqueous solutions were mixed in a beaker. The beaker was covered by polyethene film, placed in a electrical oven and heated to 90 °C and kept at the temperature for 12 h. The formed precipitate was filtered, washed thoroughly with distilled water, and dried at 90 °Cfor 12 h. Thus, zinc carbonate hydroxide nanobelts were obtained. ZnO nanowires were prepared as follows. The sample of zinc carbonate hydroxide nanobelts was heated to 300 °C, and remained at 300 °C for 5 h.

ZnO nanocrystals were prepared according to the following precedure. 1.33 mol $L^{-1}$ $Na_2CO_3$ aqueous solution was added to 100 mL of 0.2 mol $L^{-1}$ $Zn(NO_3)_2$ aqueous solution under magnetic stirring until pH is 6−7. The formed precipitate was filtered, washed thoroughly with distilled water, and dried at 100 °C for 2 h. The dried sample was heated to 350 °C in a muffle furnace and remained at 350 °C for 5 h.

**2.2. Characterization.** X-ray diffraction (XRD) patterns were observed on a Rigaku Dmax X-ray diffractometer using Cu K$\alpha$ radiation. Scanning electron microscopy (SEM) images were obtained by using a Hitachi S-4800 scanning electron microscope. Transmission electron microscopy (TEM) images were obtained by using a JEM-100CX electron microscope. TG-DSC of the zinc carbonate hydroxide nanobelts was measured on a STA449c/3/G thermal analyzer. The steady-state photoluminescence spectra (PL) and fluorescence emission decay for the ZnO samples were recorded at room temperature on a QM/TM/NIR spectrofluorometer (PTI) by using 337 nm excitation light.

**2.3. Photocurrent and Impedance Measurements.** Nanostructured ZnO photodetector was fabricated as follows. The powder of the zinc carbonate hydroxide nanobelts was mixed with ethanol, and ultrasonicated for 30 min, then ground to slurry with an agate mortar. The obtained slurry was uniformly spread on an ITO glass substrate (1.0 cm × 2.5 cm). Another ITO glass substrate was covered on the slurry to form an ITO/the zinc carbonate hydroxide nanobelts/ITO stack. After the evaporation of ethanol, the ITO/the zinc carbonate hydroxide nanobelts/ITO stack was heated to 300 °C in a muffle furnace, and remained at 300 °C for 5 h to form the ITO/ZnO nanowirs/ITO sandwich stack. The ITO/ZnO nanocrystals/ITO sandwich stack was fabricated by a precedure similar to the ITO/ZnO nanowirs/ITO sandwich stack, in which the precipitate powder obtained by the reaction between $Na_2CO_3$ and $Zn(NO_3)_2$ as described above is used instead of zinc carbonate hydroxide nanobelts, followed by calcination at 350 °C for 5 h. The *I*−*V* curves and transient response of photocurrent for the nanostructured ZnO photodetectors in air at ambient temperature were measured on an electrochemical analyzer (CHI750). A 365 nm LED UV lamp with controllable output UV intensity (UPEC Π UV LED) was used as a light source. The UV intensity of the UV lamp was measured with an UV-A radiometer.

Impedance spectroscopy was recorded for the UV photodetectors on an electrochemical analyzer (CHI750) in a frequency range of 0.1 to $10^6$ Hz at an ac amplitude of 0.5 V.

## 3. RESULTS AND DISCUSSION

**3.1. Characterization of Zinc Carbonate Hydroxide Nanobelts.** Zinc carbonate hydroxide nanobelts were prepared by the hydrolysis of zinc acetate aqueous solution in the presence of urea at 90 °C as described in the Experimental Section. Figure 1 shows XRD patterns of the as-synthesized

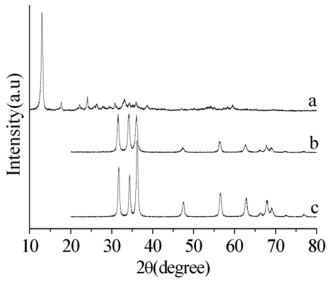


**Figure 1.** XRD patterns of (a) zinc carbonate hydroxide nanobelts, (b) ZnO nanowires and (c) ZnO nanocrystals.

zinc carbonate hydroxide sample. The observed diffraction peaks can be indexed to those of $Zn_5(CO_3)_2(OH)_6{\cdot}nH_2O$ (PDF19−1458). The average crystal size of the zinc carbonate hydroxide is determined to be 46.8 nm according to Scherrer formula ($L = 0.89\lambda/\beta\cos\theta$) at $2\theta = 13.3°$. SEM image (Figure 2a) reveals that the as-synthesized zinc carbonate hydroxide

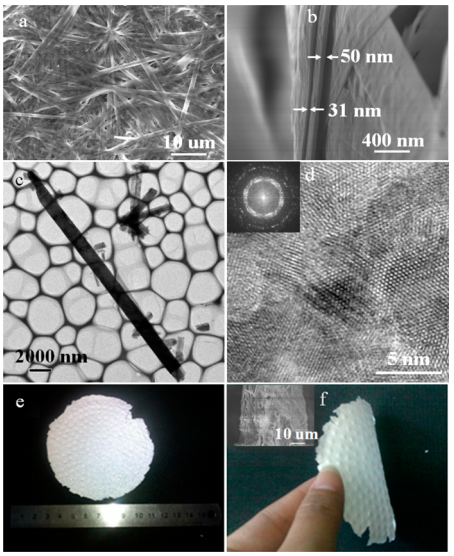


**Figure 2.** Morphology of zinc carbonate hydroxide nanobelts: (a) SEM, (b) cross-section SEM, (c) TEM, (d) HRTEM and (inset) its corresponding FFT, (e, f) camera pictures of free-standing paper, and (inset in f) cross-section SEM of the free-standing paper.

sample is characterized by a morphology of interwoven nanobelts with lengths of tens micrometers and uniform widths of 0.53−2.16 $\mu$m (Figure 2a). It can be seen from a cross-section SEM image of the zinc carbonate hydroxide nanobelts that they have uniform thickness of ∼50 nm (Figure 2b). Figure 2c presents TEM image of a selected zinc carbonate hydroxide nanobelt. It has a width of 1.4 $\mu$m and a length of 20 $\mu$m, which is in agreement to the observation of SEM. HRTEM image and its corresponding local fast-Fourier transformation (FFT) pattern reveal that the zinc carbonate hydroxide nanobelt is polycrystalline (Figure 2d). Very interestingly, after filtering, washing and drying at ambient temperature of the precipitate obtained by the hydrolysis of zinc acetate aqueous solution in the presence of urea, a freestanding film of the zinc carbonate hydroxide nanobelts is easily peeled off from a filter paper (Figure 2e, f). The circular freestanding film of the zinc carbonate hydroxide nanobelts has a diameter of 8.4 cm and thickness of ∼48 $\mu$m and remains intact and flexible even after it is intentionally bent.

Figure 3 presents TG-DSC curves of the zinc carbonate hydroxide nanobelts. There is observed a small endothermic

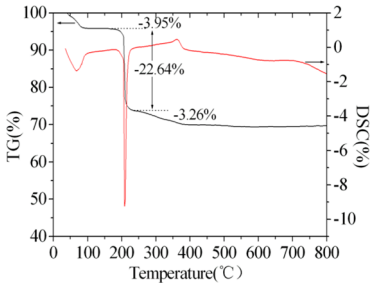


**Figure 3.** TG-DSC curves of the zinc carbonate hydroxide nanobelts.

peak around 68.7 °C accompanied by a weight loss of 3.95%, which is ascribed to the desorption of physically adsorbed water. When the temperature increases to 209.2 °C, a strong endothermic peak accompanied by a weight loss of 22.64% is observed. This peak is attributed to the decomposition of zinc carbonate hydroxide. There is another weight loss of 3.26% at the temperature range of 210−400 °C and no other weight loss is observed when temperature is above 400 °C. This observation indicates that the decomposition of the zinc carbonate hydroxide to ZnO is complete below 400 °C.

**3.2. Formation Mechanism.** The formation of zinc carbonate hydroxide is initiated by the slow reaction between urea and water. Urea plays an important role during the solution reaction process. It is used as a dual-role agent, not only as a provider of carbonate but also as a slow-released pH adjusting agent.[32]

$$CO(NH_2)_2 + 3H_2O = 2NH_3{\cdot}H_2O + CO_2 \quad (1)$$

$$NH_3{\cdot}H_2O = NH_4^+ + OH^- \quad (2)$$

$$CO_2 + 2OH^- = CO_3^{2-} + H_2O \quad (3)$$

$$5Zn^{2+} + 6OH^- + 2CO_3^{2-} + nH_2O = Zn_5(CO_3)_2(OH)_6{\cdot}nH_2O \quad (4)$$

During the initial stage, the decomposition of urea produces $OH^-$ and $CO_3^{2-}$ anions according to eqs 1−3. The $OH^-$ and $CO_3^{2-}$ anions further react with the $Zn^{2+}$ ions, which are released by $ZnAc_2$ in the solution, and form zinc carbonate hydroxide according to eq 4. As the reaction proceeds, the concentration of zinc carbonate hydroxide in the solution becomes saturated, and hence the crystal nuclei of zinc carbonate hydroxide are formed in the solution. The formed zinc carbonate hydroxide crystal nuclei subsequently grow, accompanied by the progressive hydrolysis of urea.

Zinc carbonate hydroxide ($Zn_5(CO_3)_2(OH)_6$) is monoclinic with $a$ = 13.62 Å, $b$ = 6.30 Å, $c$ = 5.42 Å, and $\beta = 95^0.50$, space group $C2/m$. It has a layered crystal structure composed of zinc in both octahedral and tetrahedral coordination in the ratio 3:2. The octahedral zinc atoms form part of C6 type sheet with holes, which are distributed on rectangular 6.3 × 5.4 net. Zinc atoms in tetrahedral coordination occur above and below these holes. The positively charged complex layers parallel to {100} plane are held together by $CO_3^{2-}$ groups to keep charge neutrality.[33] The layer {100} plane of zinc carbonate hydroxide mainly composed of zinc atoms shows relative hydrophobicity.[34] However, the {002} plane, which is vertical to the layer {100} plane, exhibits hydrophilicity as it comprises six polar hydroxyl groups.[34] Therefore, in the process of the growth of the crystal nuclei of zinc carbonate hydroxide, the hydrophilic ions of $CO_3^{2-}$, $OH^-$, and $Zn^{2+}$ preferably attack the crystal of zinc carbonate hydroxide from its hydrophilic {002} plane rather than its hydrophobic {100} plane, resulting the formation of hydroxide zinc carbonate nanobelts.

**3.3. Characterization of ZnO Nanowires.** According to the TG/DSC results, we prepared ZnO nanowires by calcining the zinc carbonate hydroxide nanobelts at 300 °C for 5 h under normal atmospheric conditions. XRD analysis shows that the thermal decomposition of the zinc carbonate hydroxide nanobelts gives rise to the formation of a pure hexagonal ZnO phase with a wurtzite structure (Figure 1b). The average crystal size of the ZnO sample is determined to be 15.7 nm according to Scherrer formula at $2\theta$ = 36.0°. SEM images reveals that the calcination leads to the transform of the zinc carbonate hydroxide nanobelts to ZnO nanowires (Figure 4a).

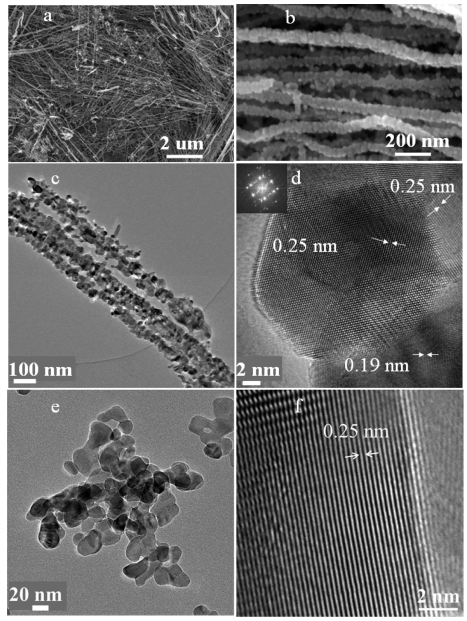


**Figure 4.** Morphology of the ZnO samples: (a) SEM, (b) high-magnification SEM, (c) TEM, (d) HRTEM and (inset) its corresponding FFT of ZnO nanowires, and (e) TEM and (f) HRTEM of ZnO nanocrystals.

The high-magnification SEM image in Figure 4b shows that ZnO nanowires are long chains of closely attached nanoparticles. The ZnO nanowires have diameters of 37−79 nm, and lengths of tens of micrometer. The morphology and microstructure of the ZnO nanowires were further characterized by TEM and HRTEM (Figure 4c, d). TEM image confirms that ZnO nanowire is long chain of closely attached nanoparticles with size of 11−46 nm. Its HRTEM image reveals that each of nanoparticles is ZnO nanocrystal, which partially overlaps with neighboring ZnO nanocrystals. This observation indicates that the ZnO nanowires exhibit unique nanostructure characterized by long chains of closely attached ZnO nanocrystals with ZnO/ZnO nanocrystal junctions. It is worth noting that the larger circular freestanding film of zinc carbonate hydroxide nanobelts transforms into small freestanding sheets of ZnO nanowires after calcination at 300 °C


dx.doi.org/10.1021/am401533w | ACS Appl. Mater. Interfaces 2013, 5, 5861−5867

for 5 h. The freestanding sheets of ZnO nanowires are fragile and easily broken if they are intentionally bent.

**3.4. UV Photodetector.** We fabricated a ZnO nanowire-based UV photodetector with ITO/ZnO nanowires/ITO sandwich stack. The photocurrent performances of the unique ZnO nanowire UV photodetector are shown in Figure 5. Figure

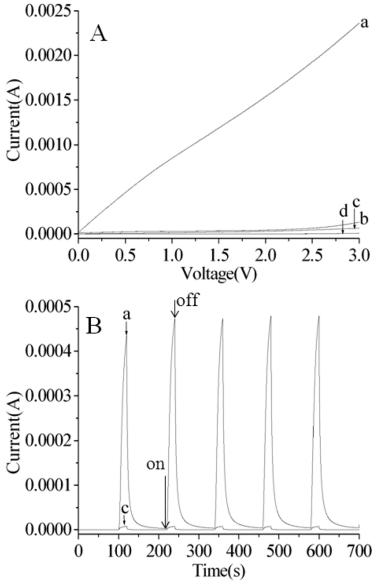


**Figure 5.** (A) $I-V$ curves of the UV photodetectors in the dark and under continuous UV irradiance of 120 mW cm$^{-2}$: ZnO nanowires (a) under UV illumination and (b) in the dark, ZnO nanocrystal (c)s under UV illumination and (d) in the dark. (B) The photoresponse switching behavior of the UV photodetectors of the (a) ZnO nanowires and (c) ZnO nanocrystals under the UV irradiance of 120 mW cm$^{-2}$ and applied voltage of 0.5 V.

5a shows the $I-V$ curves of the photodetector in the dark (black) and under continuous illumination of LED UV lamp ($\lambda$ = 365 nm). The photocurrent significantly increases with the applied voltage, whereas the dark current slowly increases with the applied voltage. Figure 5b illustrates the photoresponse switching behavior of the ZnO nanowire UV photodetector under the UV irradiance of 120 mW cm$^{-2}$ and the applied voltage of 0.5 V. It is evident that the ZnO nanowires can be reversibly switched between the low and the high conductivity state as the UV lamp is switched on and off. A low conductivity in the dark is caused by the depletion layer formed near the surface by adsorbed oxygen molecules and free electrons in the n-type semiconductor [$O_2(g) + e^- \rightarrow O_2^-(ad)$]. Under illumination with photons with energy greater than the bandgap of ZnO, photogenerated holes migrate to the surface and discharge the negatively charged adsorbed oxygen ions through surface electron–hole recombination [$h^+ + O_2^- \rightarrow O_2(g)$]. Simultaneously, the photogenerated electrons significantly increase the conductivity of the ZnO nanowires.[20,21] Under the UV irradiance of 120 mW cm$^{-2}$ and low applied voltage of 0.5 V, a peak photoresponse current of 0.436 mA is achieved for the ZnO nanowire UV photodetector. The peak photoresponse current increases to 2.36 mA when 3 V voltage is applied (Figure 5a), which is large enough to be detected by a passive mechanical ammeter. The on/off current ratio of the ZnO nanowire UV photodetector is as high as $1.26 \times 10^3$. Its photoresponse rise time is 19.6 s, and its recovery time ($\tau$), defined as the time for the photoresponse current to drop to 1/e (37%) of the maximum photoresponse current,[25] is 2.5 s. A slight increase of the photoresponse current of ZnO nanowire after first circle on/off UV irradiation (Figure 5) is probably due to the following reason: After the first switching-on of the UV lamp, the well established adsorption/desorption equilibrium of $O_2$ molecules is destroyed, resulting in the desorption of the adsorbed $O_2$ molecules on ZnO nanowires due to discharging of the negatively charged adsorbed oxygen ions by photogenerated holes. The desorption of $O_2$ molecules leads to a decrease in the depletion layer near the surface of ZnO nanowires, thus an increase of free electron concentration on the surface of ZnO nanowires. The short interval time (120 s) of switching on/off UV irradiation (Figure 5) is probably insufficient for the adsorption/desorption re-equilibrium of $O_2$ molecules, resulting in a slight increase of the photoresponse current of ZnO nanowires after first circle on/off UV irradiation.

Figure 6 shows the photoresponse switching behavior of the ZnO nanowire UV photodetector under different UV intensity

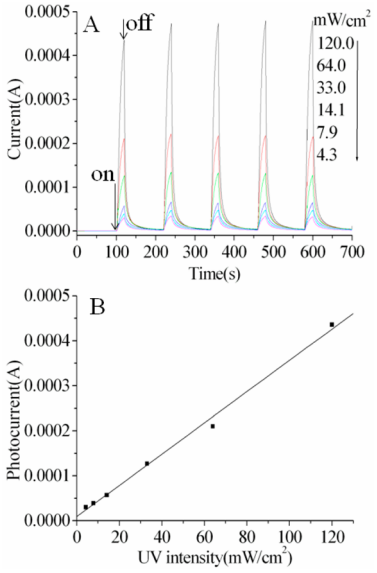


**Figure 6.** (A) Photoresponse switching behavior and (B) the peak photoresponse current versus UV intensity of the ZnO nanowire UV photodetector under different UV intensity at the applied voltage of 0.5 V.

at the applied voltage of 0.5 V. Increasing UV intensity leads to a gradual increase of photoresponse current. The peak photoresponse current versus UV intensity at the applied voltage of 0.5 V is plotted in Figure 6b. As can be seen from Figure 6b, there is very good linear relationship between UV intensity and peak photoresponse current. These results suggest that the ZnO nanowires composed of closely attached ZnO nanocrystals can be used as a highly sensitive ratiometric UV photodetector. As the ZnO nanowires are long chains of closely attached ZnO nanocrystals with size of 11–46 nm, to make comparison with the ZnO nanowire UV sensor, we fabricated an isolated ZnO nanocrystals-based UV photodetector with the procedure similar to the ZnO nanowire UV photodetector. The ZnO nanocrystals were prepared by precipitation method using $Zn(NO_3)_2$ and $Na_2CO_3$ as reactants, followed by calcination at 350 °C as described in the Experimental Section. It has a hexagonal wurtzite ZnO structure (Figure 1c). The average crystal size of ZnO nanocrystals is determined to be 20.9 nm

according to Scherrer formula, which is close to that of the ZnO nanowire (15.7 nm). TEM and HRTEM images reveal that ZnO nanocrystals are composed of 11.8−39.7 nm nanoparticles, each of which is ZnO nanocrystal (Figure 4e, f). The *I*−*V* curves and the photoresponse switching behavior of the ZnO nanocrystal UV photodetector were characterized by the same measurement procedures. The photoresponse current of the ZnO nanocrystal UV photodetector in the applied voltage range of 0 to 3.0 V is much lower than that of the ZnO nanowire UV photodetector (Figure 5a). From the photoresponse switching behavior of the ZnO nanocrystal UV photodetector under the UV irradiance of 120 mW $cm^{-2}$ and the applied voltage of 0.5 V (Figure 5b), its increase time (19.6s) and recovery time (0.9 s) are comparable to the corresponding those of the ZnO nanowire photodetector. However, the peak photoresponse current of the ZnO nanocrystal UV photodetector is only $7.84 \times 10^{-6}$ A, which is 56 times lower than that of the ZnO nanowire photodetector (0.436 mA). The on/off current ratio of the ZnO nanocrystal UV photodetector (34.8) is 36 times smaller than that of the ZnO nanowire photodetector ($1.26 \times 10^3$).

For UV photodetector based on polycrystalline ZnO thin film, a slow response time ranging from a few minutes to several hours is commonly observed.[25] The photodetectors of ZnO single nanowire or nanobelt usually show high on/off current ratio and fast response time, but their photoresponse current is very low (at ∼nA level).[22,25,26] Although the UV photoresponse currents of ZnO single nanowire photodetectors could be significantly improved by various strategies such as the decoration of ZnO nanowire with Au, Ag nanoparticles,[26,27] the formation of ZnO nanowire or nanobelt composite with $SnO_2$ or ZnS,[24,28,29] and the surface functionalization of ZnO nanobelt with polymer,[30] etc., they are generally at approximately the microamp level. The photodetectors of ZnO nanorod or nanowire array vertically aligned on larger-area substrate (∼$cm^2$) show much higher photoresponse current (at ∼$\mu$A level) than ZnO single nanorod and nanowire, but their on/off current ratio is relatively low (∼100) and recovery time is quite slow.[31,35] The formation of ZnO nanorod array/agarose gel film heterojunction[31] and the integration of multiple ZnO nanowires connected in parallel on substrate (∼$cm^2$) with Ag interdigitated transducer (IDT)-type electrodes[25] could increase both UV photoresponse currents (at ∼mA level) and on/off current ratio. Therefore, the present UV photodetector of the ZnO nanowires is among the best UV photodetection performance evidenced by its large photoresponse current (∼mA), high on/off current ratio (∼1000), and relative fast recovery time (2.5s).

To reveal why the unique ZnO nanowires exhibit much higher photoresponse currents and on/off current ratio than the ZnO nanocrystal, the two samples were characterized by steady-state photoluminescence, fluorescence decay and impedance measurement. Upon UV excitation of ZnO by light absorption with energy equal to or greater than the band gap of the semiconductor, electrons are excited from the valence band to the conduction band. The photogenerated electrons (e) and holes (h) migrate from bulk to surface, then to adjacent ZnO nanocrystals through the interface or boundary, and finally to electrodes. In competition with charge transfer is e−h recombination that usually occurs in bulk defects or on surface defects.[36,37] Therefore, the photoresponse current of the ZnO samples is affected by the e−h recombination and migration resistance.

PL is a sensitive technique to probe the e−h recombination. As shown in Figure 7A, The PL emission spectra of the two

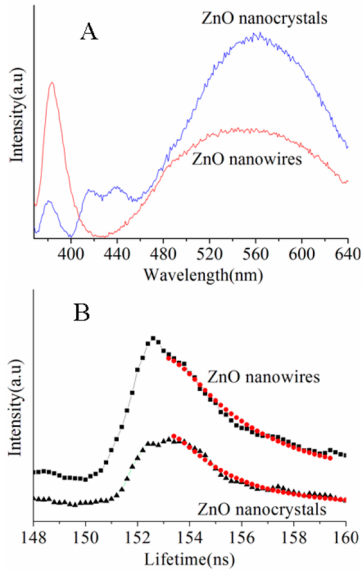


**Figure 7.** (A) Steady-state photoluminescence and (B) fluorescence emission decay for the ZnO samples: The excitation wavelength was 337 nm, and the fluorescence emission was recorded at 560 nm. The red dotted lines are the fitting curve: $R^2$ for the ZnO nanowires and ZnO nanocrystals is 0.9904 and 1.09, respectively.

ZnO samples consist of two emission bands: a sharp transition in the UV and a broad band in the visible range (400−700 nm). The narrow UV emission band is due to the excitonic recombination of electrons near the conduction band with holes near the valence band. The visible emissions are due to transition in defect states.[38,39] The two ZnO samples exhibit the strongest yellow emission around 560 nm, which are attributed to the defects of oxygen interstitials.[40,41] This observation indicates that oxygen interstitials are the dominant defects in the two ZnO samples. Two small emissions around 415 and 440 nm are observed for the ZnO nanocrystals, which are attributed to that the recombination of electrons from CB edge (tail states or shallow traps) with surface-defect-related states such as deep-acceptor levels for holes.[38,39] Compared to the ZnO nanowires, the ZnO nanocrystals exhibit much strong visible emission, suggesting that the ZnO nanocrystals have higher concentration of defects as recombination centers than the ZnO nanowires.[38,39] This result reveals that upon UV irradiation, more photogenerated charge carriers in the ZnO nanowires could migrate from the bulk to the surface, resulting in its higher separation efficiency of photogenerated electrons and holes as compared to the ZnO nanocrystals.

The recombination dynamics of photogenerated electrons and holes through the dominant defect states of the two ZnO samples were probed by fluorescence emission decay recorded at 560 nm by using 337 nm excitation light. Figure 7B shows the fluorescence decay of the two ZnO samples. The fluorescence decay can be fitted well with a single-exponential curve. The ZnO nanowires have a longer fluorescence lifetime (2.90 ns) than the ZnO nanocrystals (1.98 ns), suggesting that the photogenerated electrons and holes in the former have more probability to migrate to the electrode than those in the latter at the applied voltage (e.g., 0.5 V).

The migration resistance of photogenerated charge carriers was studied by measuring their impedance of the two ZnO samples under the UV irradiance of 120 mW $cm^{-2}$. As shown in Figure 8, the resistance of the ZnO nanocrystals is much higher

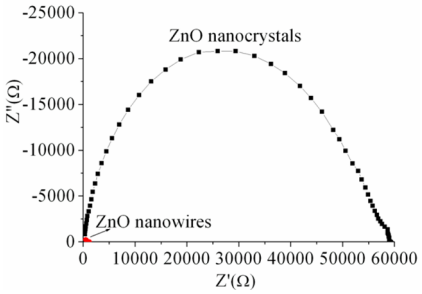


**Figure 8.** Impedance of ZnO nanowires and ZnO nanocrystals under under the UV irradiance of 120 mW $cm^{-2}$.

than that of the ZnO nanowires. The reason is as follows. The ZnO nanocrystals composed of loosely packed ZnO nanocrystals exhibit unfavorable transport characteristics in terms of the photogenerated charge carriers due to the trap-mediated hopping process of charge carriers in the nanocrystals and the tunneling of the charge carriers between adjacent nanocrystals.[22,42,43] In contrast, the ZnO nanowires are composed of long chains of closely attached ZnO nanocrystals with very good ZnO/ZnO nanocrystal junctions, in which photogenerated electrons and holes can be transferred efficiently among the adjacent ZnO nanocrystals.[22] Therefore, the superior on/off current ratio and photoresponse current of the ZnO nanowires over the ZnO nanocrystals is attributed to its lower e–h recombination and migration resistance because of its unique nanostructures.

## 4. CONCLUSIONS

In summary, zinc carbonate hydroxide nanobelts are prepared by the hydrolysis of zinc acetate aqueous solution in the presence of urea at 90 °C. The zinc carbonate hydroxide nanobelts can be facilely self-assembled in a circular flexible freestanding film. The calcination of the zinc carbonate hydroxide nanobelts at 300 °C under normal atmospheric conditions results in the formation of ZnO nanowires. The ZnO nanowires exhibit unique nanostructure characterized by long chains of closely attached ZnO nanocrystals with ZnO/ZnO nanocrystal junctions. The ZnO nanowire-based UV photodetector exhibit much higher photoresponse currents (at the milliampere level) and on/off current ratio (~1000) than the ZnO nanocrystal-based UV photodetector due to its unique nanostructure. The present work provides a novel approach to improve the photoresponse current and on/off current ratio of nanostructured ZnO UV photodetector.

## AUTHOR INFORMATION

### Corresponding Author

*E-mail: liyuanzhi66@hotmail.com.

### Notes

The authors declare no competing financial interest.

## ACKNOWLEDGMENTS

This work was supported by National Basic Research Program of China (2009CB939704), National Natural Science Foundation of China (21273169), Innovative Research Team Project of Hubei Province (2010CDA070), and the Fundamental Research Funds for the Central Universities.

## REFERENCES

(1) Bao, J.; Zimmler, M. A.; Capasso, F.; Wang, X.; Ren, Z. F. *Nano Lett.* **2006**, *6*, 1719–1722.
(2) Mariano, A. Z.; Jiming, B.; Federico, C.; Sven, M.; Carsten, R. *Appl. Phys. Lett.* **2008**, *93*, 051101.
(3) Wang, X. D.; Song, J. H.; Liu, J.; Wang, Z. L. *Science* **2007**, *316*, 102–105.
(4) Law, M.; Greene, L. E.; Johnson, J. C.; Saykally, R.; Yang, P. *Nat. Mater.* **2005**, *4*, 455–459.
(5) Yang, X.; Wolcott, A.; Wang, G.; Sobo, A.; Fitzmorris, R. C.; Qian, F.; Zhang, J. Z.; Li, Y. *Nano Lett.* **2009**, *9*, 2331–2336.
(6) Zhang, H. J.; Wu, R. F.; Chen, Z. W.; Liu, G.; Zhang, Z. N.; Jiao, Z. *CrystEngComm* **2012**, *14*, 1775–1782.
(7) Yang, K.; She, G. W.; Wang, H.; Ou, X. M.; Zhang, X. H.; Lee, C. S.; Lee, S. T. *J. Phys. Chem. C* **2009**, *113*, 20169–20172.
(8) Lu, F.; Cai, W. P.; Zhang, Y. G. *Adv. Funct. Mater.* **2008**, *18*, 1047–1056.
(9) Li, Y. Z.; Xie, W.; Hu, X. L.; Shen, G. F.; Zhou, X.; Xiang, Y.; Zhao, X. J.; Fang, P. F. *Langmuir* **2010**, *26*, 591–597.
(10) Luo, L.; Zhang, Y. F.; Mao, S. S.; Lin, L. W. *Sensor. Actuat. A-Phys.* **2006**, *127*, 201–206.
(11) Chang, S. P.; Chen, K. J. *J. Nanomater.* **2012**, 602398.
(12) Jin, Y. Z.; Wang, J. P.; Sun, B. Q.; Blakesley, J. C.; Greenham, N. C. *Nano Lett.* **2008**, *8*, 1649–1653.
(13) Chen, M.; Hu, L. F.; Xu, J. X.; Liao, M. Y.; Wu, L. M.; Fang, X. S. *Small* **2011**, *7*, 2449–2453.
(14) Wang, X.; Liao, M. Y.; Zhong, Y. T.; Zheng, J. Y.; Tian, W.; Zhai, T. Y.; Zhi, C. Y.; Ma, Y.; Yao, J. N.; Bando, Y.; Golberg, D. *Adv. Mater.* **2012**, *24*, 3421–3424.
(15) He, J. H.; Lin, Y. H.; McConney, M. E.; Tsukruk, V. V.; Wang, Z. L. *J. Appl. Phys.* **2007**, *102*, 084303.
(16) Prades, J. D.; Jimenez-Diaz, R.; Hernandez-Ramirez, F.; Fernandez-Romero, L.; Andreu, T.; Cirera, A.; Romano-Rodriguez, A.; Cornet, A.; Morante, J. R.; Barth, S.; Mathur, S. *J. Phys. Chem. C* **2008**, *112*, 14639–14644.
(17) Ahn, S. E.; Lee, J. S.; Kim, H.; Kim, S.; Kang, B. H.; Kim, K. H.; Kim, G. T. *Appl. Phys. Lett.* **2004**, *84*, 5022–5024.
(18) Ji, L. W.; Peng, S. M.; Su, Y. K.; Young, S. J.; Wu, C. Z.; Cheng, W. B. *Appl. Phys. Lett.* **2009**, *94*, 203106.
(19) Yang, Q.; Guo, X.; Wang, W. H.; Zhang, Y.; Xu, S.; Lien, D. H.; Wang, Z. L. *ACS Nano* **2010**, *4*, 6285–6291.
(20) Soci, S.; Zhang, A.; Xiang, B.; Dayeh, S. A.; Aplin, D. P. R.; Park, J.; Bao, X. Y.; Lo, Y. H.; Wang, D. *Nano Lett.* **2007**, *7*, 1003–1009.
(21) Kind, H.; Yan, H.; Messer, B.; Law, M.; Yang, P. D. *Adv. Mater.* **2002**, *14*, 158–160.
(22) Seong, H. J.; Yun, J. G.; Jun, J. H.; Cho, K.; Kim, S. S. *Nanotechnology* **2009**, *20*, 245201.
(23) Lieber, C. M.; Wang, Z. L. *MRS Bull.* **2007**, *32*, 99–108.
(24) Hu, L. F.; Yan, J.; Liao, M. Y.; Xiang, H. J.; Gong, X. G.; Zhang, L. D.; Fang, X. S. *Adv. Mater.* **2012**, *24*, 2305–2309.
(25) Bai, S.; Wu, W. W.; Qin, Y.; Cui, N. Y.; Bayerl, D. J.; Wang, X. D. *Adv. Funct. Mater.* **2011**, *21*, 4464–4469.
(26) Liu, K. W.; Sakurai, M.; Liao, M. Y.; Aono, M. *J. Phys. Chem. C* **2010**, *114*, 19835–19839.
(27) Lin, D. D.; Wu, H.; Zhang, W.; Li, H. P.; Pan, W. *Appl. Phys. Lett.* **2009**, *94*, 172103.
(28) Bera, A.; Basak, D. *ACS Appl. Mater. Interfaces* **2010**, *2*, 408–412.
(29) Lin, C. C.; Chen, Y. W.; Chiang, M. C.; Lee, C. H.; Tung, Y. L.; Chen, S. Y. *J. Electochem. Soc.* **2010**, *157*, H227.
(30) Lao, C. S.; Park, M. C.; Kuang, Q.; Deng, Y. L.; Sood, A. K.; Polla, D. L.; Wang, Z. L. *J. Am. Chem. Soc.* **2007**, *129*, 12096–12097.
(31) Mandal, L.; Deo, M.; Yengantiwar, A.; Banpurkar, A.; Jog, J.; Ogale, S. *Adv. Mater.* **2012**, *24*, 3686–3691.
(32) Zhou, X. F.; Hu, Z. L.; Fan, Y. Q.; Chen, S.; Ding, W. P.; Xu, N. P. *J. Phys. Chem. C* **2008**, *112*, 11722–11728.

(33) Ghose, S. *Acta Crystallogr.* **1964**, *17*, 1051−1057.
(34) Su, B.; Li, M.; Shi, Z. Y.; Lu, Q. H. *Langmuir* **2009**, *25*, 3640−3645.
(35) Manekkathodi, A.; Lu, M. Y.; Wang, C. W.; Chen, L. J. *Adv. Mater.* **2010**, *22*, 4059−4063.
(36) Yates, J. T., Jr. *Chem. Rev.* **2006**, *106*, 4428−4453.
(37) Kong, M.; Li, Y. Z.; Chen, X.; Tian, T. T.; Fang, P. F.; Zheng, F.; Zhao, X. J. *J. Am. Chem. Soc.* **2011**, *133*, 16414−16417.
(38) Layek, A.; De, S.; Thorat, R.; Chowdhury, A. *J. Phys. Chem. Lett.* **2011**, *2*, 1241−1247.
(39) Layek, A.; Manna, B.; Chowdhury, A. *Chem. Phys. Lett.* **2012**, *539*−*540*, 133−138.
(40) Wu, X. L.; Siu, G. G.; Fu, C. L.; Ong, H. C. *Appl. Phys. Lett.* **2001**, *78*, 2285−2287.
(41) Li, D.; Leung, Y. H.; Djurisic, A. B.; Liu, Z. T.; Xie, M. H.; Shi, S. L.; Xu, S. J.; Chan, W. K. *Appl. Phys. Lett.* **2004**, *85*, 1601−10603.
(42) Ginger, D. S.; Greenham, N. C. *J. Appl. Phys.* **2000**, *87*, 1361−1368.
(43) Kim, H.; Cho, K.; Park, B.; Kim, J. H.; Lee, J. W.; Kim, S.; Noh, T.; Jang, E. *Solid State Commun.* **2006**, *137*, 315−319.